ORIGINAL PAPER

Metamorphic reaction kinetics at anhydrous to water-saturated conditions in the binary MgO-SiO$_2$ system

M. G. Franke[1] · B. C. Schmidt[2] · R. Stalder[1] · B. Joachim-Mrosko[1]

Abstract

Reaction rims contain a wealth of information that can be used to decipher the P-T-t-X history of metamorphic and metasomatic rocks. One of the most important parameters that controls reaction rim growth is the presence of volatiles, which can affect rim thicknesses, phase stabilities and the development of rim microstructures. In this study, reaction rim growth experiments were performed between periclase and quartz at anhydrous to water-saturated conditions at 3–4 kbar and 1100–1300 °C. Controlled minute amounts of water were added through OH-doped periclase, which enabled us to perform experiments at controlled water-undersaturated conditions. At anhydrous conditions, no reaction rim formed at all implying that water acts as a catalyst, and a minimum fluid threshold is needed to initiate metamorphic reactions. At water-undersaturated conditions extremely small variations in water content are sufficient to change reaction rim growth rates by multiple orders of magnitude. This implies that reaction rims have the potential to monitor variations in the amount of water at those grain boundaries that serve as fast pathways for component transport at water-undersaturated conditions during metamorphic and metasomatic reactions in natural systems, allowing them to be used as sensitive "geohygrometers". Additionally, the effect of water on relative layer thicknesses may provide an application for reaction rim microstructures to be used as new physico-chemical gauges that will allow us to discriminate between water-undersaturated and water-saturated conditions during metamorphic events.

Introduction

Metamorphic coronas and reaction rims are examples of net-transfer reactions, in which pre-existing mineral phases react to form new phases. The dynamic of this process is primarily influenced by changes in temperature, a change in the chemical composition of a system, and/or by the presence of volatile components. This means that the effect of volatiles

on reaction rim growth can be quantified in a well-calibrated system, which not only allows to study in detail the effect of fluids during metamorphism and metasomatism but also the corresponding mechanisms that control re-equilibration at different fluid–rock fractions (Franke and Joachim-Mrosko 2022). This also implies that many features of multi-component natural reactions rims, such as the overall rim thickness, the layer sequence and the internal microstructure contain valuable information about the respective rim growing conditions and in particular the fluid abundance and composition during fluid-mediated metamorphism and metasomatism (Joesten 1977). The availability of fluids, in particular H$_2$O, is in fact one of the most important parameters that controls the kinetics of metamorphic and metasomatic reactions. Their presence may determine the start and succession of these reactions, where fluids may catalyse reactions and through this lower the free energy of the system (Rubie 1986; Austrheim 1987; Putnis and Austrheim 2010; Schorn and Diener 2017; Mindaleva et al. 2020). An example is

✉ M. G. Franke
Mees.Franke@uibk.ac.at

1 Faculty of Geo- and Atmospheric Sciences, Institute of Mineralogy and Petrography, University of Innsbruck, Innrain 52f, 6020 Innsbruck, Austria

2 Department for Mineralogy and Petrology, Geoscience Centre, Georg-August-University Göttingen, Goldschmidtstrasse 1, 37077 Göttingen, Germany

eclogitization of pre-cambrian anorthositic granulites of the Bergen Arcs in Western Norway, where a cm-thick band of eclogite developed along a shear plane associated with fluid migration cuts through a granulite rock (Austrheim 1987). Examples of fluid-mediated metamorphism on a regional scale involve the albitization of km-wide terranes in the Olary Domain, South Australia where several stages of fluid infiltration are held responsible for this alteration (Clark et al. 2005). Even at water-undersaturated conditions, re-equilibration of initially metastable granulite rocks to eclogite has been described where minute amounts of water (10-100 s ppm) and a water activity (a_{H2O}) as low as 0.15 (Schorn and Diener 2017) are sufficient to catalyse the reaction. Thermodynamic modelling shows that during prograde stages of metamorphism, a minimum water threshold is necessary to form new minerals, while relict, anhydrous porphyroblasts remain metastable at fluid deficient conditions even during exhumation (Tursi 2022). These observations not only reinforce the idea that fluids are essential for triggering metamorphic and metasomatic reactions on a local and regional scale, but also affect the mineral assemblage and reaction textures. Growth kinetics of reaction rims were repeatedly investigated over a wide range of P–T conditions and are in general well understood, particularly at nominally dry conditions. Examples include the growth of spinel between periclase and corundum in the binary MgO-Al_2O_3 system (Carter 1961; Rossi and Fulrath 1963; Whitney and Stubican 1971; Watson and Price 2002; Götze et al. 2010; Keller et al. 2010), the system $CaCO_3$–SiO_2 where wollastonite grows between calcite and quartz (Milke and Heinrich 2002), the binary MgO–SiO_2 (Brady and McCallister 1983; Yund 1997; Fisler et al. 1997; Milke et al. 2001, 2007, 2009; Abart et al. 2004; Götze et al. 2010; Gardés et al. 2011), and the ternary CaO–MgO–SiO_2 (CMS) system (Joachim et al. 2011, 2012). However, it was not possible to quantify the amount of fluids in these experiments when they were present in extremely small concentrations, while it had been demonstrated earlier that fluids not only play a catalytic but also a thermodynamic role in determining the course of a metamorphic reaction (Putnis and Austrheim 2010). Consequently, investigating and quantifying the impact of water on the kinetics of net-transfer reactions and the underlying mechanisms involved is essential to understand its significance in metamorphic processes.

The study of mechanisms governing reaction rim growth is well established. Reaction rim growth follows a parabolic pattern, if the effective diffusion coefficient remains constant over time, (Fisher 1978). Multiple experimental studies have confirmed this parabolic growth, emphasizing the important role of diffusion-controlled rim growth dynamics (Zaraysky et al. 1989; Liu et al. 1997). In some cases, the growth of a reaction rim can deviate from this parabolic behaviour for example due to grain coarsening as reaction proceeds, which decreases overall rim growth rates over time (Gardés et al. 2011). Additionally, even if overall growth rates conform with the parabolic model, various studies have documented slower rim growth at the onset of reaction rim growth (Yund 1997; Milke et al. 2007; Joachim et al. 2011). These observations align with thermodynamic models proposing that initial growth stages are invariably interface reaction-controlled due to finite interface mobilities. Subsequently, a gradual transition to diffusion-controlled growth may occur (Abart and Petrishcheva 2011).

There is a general consensus that water, or rather a hydrous fluid phase, increases the mobility of chemical components along grain boundaries, which has been experimentally demonstrated with reaction rim growth experiments in both the binary MgO–SiO_2 (Yund 1997; Milke et al. 2001, 2007, 2009, 2013; Gardés et al. 2011, 2012; Incel et al. 2022) and the ternary CMS system (Joachim et al. 2011, 2019; Franke and Joachim-Mrosko 2022). In turn, these studies can be used to categorize the effect of water on intergranular diffusivity in four regimes, that each describe a pathway for mass transfer. As a general trend, the diffusivities increase with increasing fluid-rock fraction, sorted from low to high transport kinetics as follows: (1) "water-absent": diffusion along effectively dry grain boundaries. (2) "water-undersaturated": diffusion along water-undersaturated grain boundaries. (3) "water-saturated grain boundaries": the first regime occurring at fluid-saturated conditions. (4) "interconnected fluid-filled porosity": fluid-filled grain boundaries and pores start to interconnect forming new potential pathways for mass transfer (Farver and Yund 1995; Carlson 2010; Gardés et al. 2012). Re-equilibration rates obtained from reaction rim growth experiments in the MgO-SiO_2 system at "dry" (regime 1) and "wet" (regime 3) conditions are often separated by a gap of multiple orders of magnitude, defined as regime 2, where kinetics increase virtually instantaneous (Dohmen and Milke 2010; Gardés et al. 2012). As a result, kinetic data are often categorized in either a "dry" or a "wet" zone (Gardés et al. 2012). However, a quantification of the amount of water required for this transition and concomitant with that an understanding of the mechanisms how diffusivity increases with fluid-rock fraction in regime 2 is still lacking and requires experimental data that are able to bridge the gap between these two zones. These are hitherto missing.

The main obstacle to study reaction kinetics experimentally at water-undersaturated conditions is the capability to introduce defined, minute amounts of water to a closed system. Previous efforts made to investigate reaction rim growth dynamics at near dry conditions often utilize a powder matrix, resulting in the addition of hygroscopically adsorbed water (Gardés et al. 2012; Joachim et al. 2012, 2019; Franke and Joachim-Mrosko 2022; Incel et al. 2022). This in turn makes it almost impossible to keep the system

dry and simultaneously limits the capability to determine how much water was present at the start of the experiment as this depends on many factors, including but not limited to: the relative humidity, the hygroscopicity of the starting materials, the drying temperature, the total surface area, and the time it takes to prepare and seal the capsule. Especially in experiments that approach (near) "dry" conditions, small discrepancies of these variables often lead to inconsistent results due to the sensitivity of reaction rim growth at low amounts of H_2O (Joachim et al. 2019). This in turn makes fine powder experiments unsuitable to investigate the transition between "dry" and "wet" reaction kinetics due to limitations to obtain anhydrous conditions and accurately determine the amount of H_2O in the system. The addition of controlled minute amounts of water to single crystals is also challenging as ppm-amounts may already be sufficient to push the system to regime 3 (Milke et al. 2013).

The aim of this study is to investigate the transition from "dry" regime 1 to "wet" regime 3 rim growth kinetics by using a new technique that enables the addition of controlled minute amounts of H_2O to an experimental setup. This will provide a significant step forward toward our understanding of how minute amounts of water affect rim growth kinetics at water-undersaturated conditions and improve our understanding of the role and significance of fluids during metamorphism.

Experimental methods

Starting materials

Dry experiments were performed using rectangular synthetic dry single crystals as starting material. In water-undersaturated experiments, controlled minute amounts of water were added by using synthetic periclase as starting material that was doped with OH-defects prior to the rim growth experiments. In water-saturated experiments, brucite powder served as water source. Reactants used in all experiments were synthetic rectangular shaped single crystals of quartz (2.5×2.5 mm wide and 0.5 mm thick) and periclase (2.25×2.25 mm wide and 1 mm thick) that were supplied by Crystec GmbH (Berlin). The initial water content of both quartz and periclase is below the FTIR detection limit (< 1 ppm H_2O). Periclase was doped with OH by annealing at water-saturated conditions. The crystals were loaded with 10 wt% of double de-ionized water in a platinum capsule that was welded shut. The sealed platinum capsules where then loaded in an Internally Heated Pressure Vessel (IHPV) and pressurized to 4 kbar at 1200 °C for 66 h. The P-T-t conditions for the doping experiments were chosen based on well-known H^+ and H_2O diffusivities in synthetic periclase (Joachim et al. 2013) with the aim to ensure a homogenous

distribution of OH-defects while minimizing the incorporation of molecular H_2O and therefore the formation of brucite precipitates in the periclase starting material (Joachim et al. 2013). Formation of such precipitates near the rim of the periclase can, however, not be fully avoided, so that these precipitates were removed after the doping experiment by polishing off approximately 200 μm from all sides of the doped periclase crystal. The homogeneous distribution of OH-defects throughout the doped periclase crystal and the complete removal of all brucite precipitates were afterwards confirmed with FTIR spectroscopy. To introduce the desired amount of water to each experiment, doped periclase crystals were chosen accordingly based on their H_2O concentration and dimensions.

Dehydration experiments

The water-release rate of the doped periclase was determined by heating the crystal in a conventional box furnace using ambient atmosphere at 1100–1300 °C. The crystal thicknesses in the annealing experiments were directly comparable to those used for rim growth experiments. Water contents were determined by FTIR spectroscopy at pre-determined time intervals depending on the drying temperature. Each crystal was dried until at least 90% of their original water content was lost. In addition, the occurrence of OH-defects was detected by IR imaging in samples IHPV-6 and IHPV-9 after the rim growth experiments to check if the starting materials and product phases contain H-related species.

Capsule preparation

For each rim growth experiment, the reactants were stacked in a platinum capsule (ID 3.6 mm, OD 4.00 mm) and compressed with pliers to hold the reactants in place. The crystals were aligned such that the whole surface area of the periclase crystal is in contact with the quartz crystal, while maintaining a consistent crystallographic orientation of the reaction surface in all experiments by using synthetic oriented starting materials (Fig. 1a). After welding, all sealed capsules were weighed before and after they were pressurised to 1 kbar in a Cold-Seal Pressure Vessel (CSPV) to check for leakage. Sample IHPV-14, which represents the driest of all experiments, was dried in a conventional oven at 120 °C for 30 min before the capsule was subsequently welded shut with a plasma welder (Table 1). For experiments that contain wt% amounts of H_2O, water was added in the form of brucite powder to the samples. This was synthesized in a cold-seal pressure vessel at 600 °C and 2 kbar for 7 days in a platinum capsule by using a synthetic MgO powder with an excess of water as starting materials. X-ray diffraction confirmed the formation of brucite, which contained trace amounts of magnesite (< 0.5 wt%). A platinum
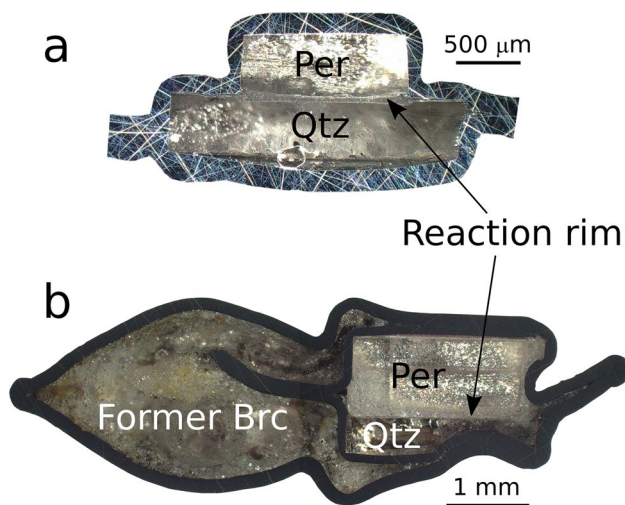
Fig. 1 Photos of experimental setups, in which water was added through **a** OH-doped periclase and **b** brucite powder. **a** Stack of a formerly OH-doped periclase single crystal and a single quartz crystal (IHPV-24). The smaller periclase facet is centred on the larger quartz crystal. The surface area of the periclase crystal that is in direct contact with quartz represents the interface area between the two crystals. **b** Double capsule containing a stack of untreated periclase in contact with a quartz single crystal (IHPV-19) in the unsealed inner capsule. The former brucite powder (now reacted to per + H_2O) surrounds the inner capsule

double-capsule was used to prevent any contact between brucite and quartz with brucite powder being located in the outer capsule (Fig. 1b). The inner capsule holding the periclase-quartz assembly was left unsealed allowing the infiltration of water that was released from the brucite during the course of the experiment.

Rim growth experiments

Rim growth experiments were performed in an IHPV at Georg-August University Göttingen, which enables the simultaneous execution of up to 8 experiments at identical P-T-t conditions. The selection of an IHPV was made to ensure a hydrostatic pressure to minimize the chance of generating cracks in the starting materials and to restrict hydrogen diffusion through the platinum capsule wall, a well-documented phenomenon in alternative methods such as piston cylinder experiments (Truckenbrodt and Johannes 1999). Three S-type thermocouples were positioned over a vertical distance of 3 cm at either side and the centre of the sample chamber to monitor the temperature. Two platinum furnace windings were independently controlled with a Eurotherm controller to minimize the temperature gradient between the thermocouples. After manually pressurizing and heating the vessel to 1–1.5 kbar and 300–400 °C, samples were heated non-isobarically with a ramp of 40 K/min, attaining pressures of 1.7–2.2 kbar once the final temperature had

been reached. After the final temperature was reached, the vessel was further pressurized with argon gas to the desired pressure of 3–4 kbar within 10 min. Further details on the run conditions of each experiment are presented in Table 1. After the runs, the samples were quenched by switching off the furnace (< 2 min to cool from 1200 to 1300 °C to about 300 °C), retrieved and embedded in epoxy. The quartz periclase stacks were polished perpendicular to their initial interface.

Analytical techniques

EMP analyses

A JEOL JXA-ISP100 electron microprobe equipped with five wavelength-dispersive spectrometers was used to determine phase compositions. For BSE imaging and analysis of mineral phases in the reaction rims, the measurement conditions were 15 kV and 10 nA. Well-known standards were used for EMPA calibration. The counting times for elements was 20 s for the peak and 10 s for the background. To determine the phase of single-layered reaction rims that were too thin to accurately measure their composition with the microprobe (< 1 µm), the relative element abundances were obtained through high resolution element mapping, which allowed us to distinguish between enstatite and forsterite (See Online Resource 1). All analyses were performed with a tungsten emitter. All rim thicknesses were determined from BSE images by averaging out at least 6 measurements between equally spaced locations to eliminate any measurement bias. The thicknesses of forsterite and enstatite in double-layered reaction rims were measured at the same location where the total rim thickness was measured. Growth rates were calculated using the measured rim thicknesses and expressed in m^2/s assuming reaction rim growth follows a parabolic rate law (see discussion for details). The exact power law that fits reaction rim growth of our experiments has not been explicitly tested and is beyond the scope of this study.

FTIR spectroscopy

The water content of periclase was determined with polarized IR absorption spectroscopy in transmission mode in the wavenumber range 3000–3800 cm^{-1}. Mid-infrared spectra were recorded at room temperature in transmission mode by using a Bruker Vertex 70 FTIR spectrometer coupled to a Hyperion 3000 microscope, nitrogen-cooled MCTD316-025 (mercury cadmium telluride) detector, a SiC globar light source, a KBr beamsplitter and a ZnSe wire grid polarizer. The beam path was continuously flushed with dry air and the periclase crystals were placed on a BaF_2 plate. In order to visualise the chemical homogeneity, the OH-distribution

Table 1 Experimental run conditions and results of all IHPV experiments performed in this study

Label	Sample type	Absolute water content [ng]	Water content per total surface area [mg/m²$_{tot}$]	water content per interface [mg/m²$_{IF}$]	t (h)	T [°C]	P [kbar]	ΔxFo [μm]	ΔxEn [μm]	Rim thickness Δx [μm]	Fo/En	Rim growth rate [log(m²/s)]
IHPV-3	SC	–	–	–	96	1100	4	n.d.	0.44 (7)	0.44 (7)	–	– 18.25 (14)
IHPV-5	SC	–	–	–	168	1100	4	n.d.	0.60 (12)	0.60 (12)	–	– 18.23 (16)
IHPV-6	D per	47.3 (46)	2.04 (20)	41.2 (40)	168	1100	4	0.45 (4)	0.69 (2)	1.14 (4)	0.64 (6)	– 17.29 (+0.49/– 0.38)[b]
IHPV-9	D per	96 (21)	3.60 (80)	40.8 (91)	66	1200	4	2.81 (8)	1.25 (7)	4.06 (6)	2.25 (17)	– 15.96 (+0.19/– 0.20)[b]
IHPV-11	SC	–	–	–	66	1200	4	n.d.	1.63 (11)	1.63 (11)	–	– 16.95 (6)
IHPV-14[a]	SC	–	–	–	168	1300	3	n.d.	n.d	n.d	–	–
IHPV-15	D per	10.9 (15)	0.50 (7)	7.35 (98)	168	1300	3	41.6 (34)	7.8 (24)	49.4 (34)	5.9 (18)	– 14.38 (6)
IHPV-16	D per	27.6 (34)	1.21 (15)	22.4 (28)	168	1300	3	41.9 (24)	5.5 (13)	47.4 (25)	8.2 (22)	– 14.42 (5)
IHPV-17	D per	4.1 (2)	0.20 (1)	3.49 (19)	168	1300	3	14.94 (46)	6.16 (53)	21.10 (73)	2.44 (25)	– 15.12 (3)
IHPV-19	br	2590·10³	70,717	511,605	168	1300	3	78.3 (74)	10.88 (77)	89.2 (80)	7.19 (38)	– 13.88 (8)[c]
IHPV-20	br	310·10³	8464	61,235	168	1300	3	75.3 (46)	8.6 (16)	83.9 (56)	9.1 (14)	– 13.94 (6)[c]
IHPV-24	D per	18.4 (18)	0.76 (7)	10.4 (10)	168	1250	3	28.1 (10)	5.81 (88)	33.91 (99)	4.95 (76)	– 14.70 (3)
IHPV-25	D per	4.8 (3)	0.23 (1)	3.40 (19)	168	1250	3	34.1 (10)	2.93 (48)	37.0 (13)	11.9 (14)	– 14.63 (3)
IHPV-26	D per	32.3 (58)	1.41 (25)	24.0 (43)	168	1250	3	30.9 (22)	6.7 (13)	37.7 (20)	4.8 (11)	– 14.61 (5)
IHPV-27	br	2810·10³	70,250	449,600	168	1250	3	88.2 (42)	11.7 (18)	99.9 (43)	7.7 (13)	– 13.78 (4)[c]
IHPV-28	br	340·10³	10,149	85,000	168	1250	3	69.1 (80)	8.2 (20)	77.4 (68)	9.0 (25)	– 14.00 (8)[c]
IHPV-31	br	320·10³	8737	63,210	68	1200	3	45.8 (33)	4.4 (10)	50.2 (39)	10.9 (22)	– 13.99 (7)[c]

Rim thicknesses represent average values of at least 6 individual measurements. Relative Fo/En were determined at the same locations and averaged afterwards. Abbreviated sample types are: *SC* untreated single crystals, *D per* doped periclase crystals, and *br* brucite powder. Absolute amount of water relative to the total sample surface area of the starting materials and the absolute amount of water relative to the interface area, which is the contact surface between periclase and quartz, is expressed as mg/m²$_{tot}$ and mg/m²$_{IF}$, respectively. Uncertainties are given in terms of 1σ

[a] oven dried at 120 °C for 1 h before the capsule was welded. All growth rates of experiments with doped periclase crystals are corrected for the time it takes for 90% of the water to be released from the periclase crystal (see discussion for details)

[b] the method to determine the error of the growth rate was similar for all experiments, but the release time of H_2O dominated the error at relatively low temperature experiments. For these experiments an upper and lower limit is provided for the growth rates that defines the starting point of the experiments at 99% and 0% H_2O release, respectively. Reported values are means and the 1 Sigma standard deviation of the means

[c] Growth rates of the brucite series either plot in regime 4a or 4b and may either follow a parabolic growth law (m²/s) or a linear rate law (m/s) (see text for details)

of selected crystals were recorded using a focal plane array (FPA) detector attached to a Hyperion 3000 IR microscope. The FPA consists of 64×64 MCTD364 detectors, resulting in 4096 simultaneously recorded spectra in an area of $170\,\mu m \times 170\,\mu m$. All spectra were automatically integrated in different spectral regions of interest near 3297 cm^{-1}, 3645 cm^{-1}, 3700 cm^{-1} providing a quick overview over the OH species-related absorption bands.

Results

FT-IR analyses of all doped periclase crystals show bands at 3297 cm^{-1} and 3645 cm^{-1}, and a layer with a thickness of several 10's of μm surrounding the crystal that shows an additional band at 3700 cm^{-1}, which can be attributed to the presence of brucite precipitates (Joachim et al. 2013). This layer was removed before the start of the actual rim growth experiments to ensure a homogeneous OH-defect distribution in all periclase starting materials, which was confirmed with FPA-imaging. The IR-band at 3297 cm^{-1} can be assigned to an OH^- stretching vibrations (V^-_{OH}) due to the presence of half-compensated cation vacancies and the band at 3645 cm^{-1} may be assigned to OH-stretching vibrations in $Ca(OH)_2$ (Phillips and Busing 1956; Gonzalez and Chen 2002; Joachim et al. 2013). The presence of $Ca(OH)_2$ may be explained by the presence of small amounts of calcium in double de-ionized water, that subsequently diffuse through the periclase crystal during the doping experiment. However, the amount of calcium required for the formation of these $Ca(OH)_2$ defects that correspond to the measured OH-stretching vibrations in the doped periclase crystal is below the detection limit of the EMP (<1 ppm). The H_2O equivalent in the OH-doped periclase crystals used as starting material for rim growth experiments in this study is in the range of 5.0(5)–15.6(35) ppm H_2O determined by using the combined absorbance of the 3297 and 3645 cm^{-1} bands and the calibration method of Libowitzky and Rossman (1997; See Online Resource 2). As both bands at 3297 cm^{-1} and 3645 cm^{-1} can unambiguously be attributed to OH-defects in the periclase structure, further investigations of the exact incorporation mechanisms are beyond the scope of this study.

Dehydration experiments show that $>90\%$ of the H_2O related species that are attributed to the bands at 3297 cm^{-1} and 3645 cm^{-1} diffuse out of the periclase within 3.5 h and 97 h at 1300 °C and 1100 °C, respectively (Fig. 2, and Online Resource 3). This has been confirmed by FT-IR analyses after the rim growth experiments in samples IHPV-6 and IHPV-9, which contained OH-doped periclase as starting material and do not show any band in the 3297–3700 cm^{-1} range in any of the starting materials or product phases.
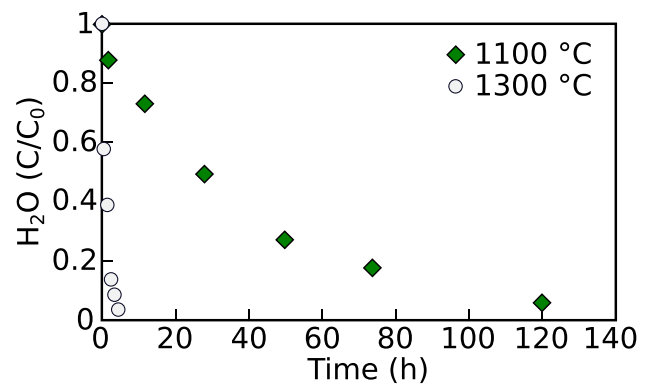

Fig. 2 Water loss of doped periclase crystals in percentage from their initial H_2O content versus time at 1100 and 1300 °C. The periclase crystals that were dried at 1100 °C and 1300 °C had an initial H_2O content of 9.3 and 8.1 ppm with a thickness of 584 and 571 μm, respectively. See Online Resource 3 for details

An overview of the experimental conditions and results is given in Table 1. High resolution BSE images of experiment IHPV-14, which was oven dried at 120 °C for 1 h prior to welding, does not show any trace of rim growth textures between the starting materials (Fig. 3a). In all other experiments, clearly observable reaction rims were formed between periclase and quartz (Fig. 3b–d). In both experiments that used undoped periclase as starting material and were not pre-dried at 120 °C, a single-layered enstatite rim formed with no sign of forsterite formation between enstatite and the periclase starting material (Fig. 3b). In all experiments that used either water-doped periclase or brucite as source of water, an enstatite-forsterite double rim formed (Fig. 3c, d). A detailed overview of the phase identification is given in Online Resource 1. In samples that contained brucite powder as source of water, the forsterite-periclase and enstatite-quartz phase boundaries are wavy (Fig. 3d). The presence of gaps (Fig. 3a–c) is caused by differential dilation during cooling and depressurization and has thus been excluded from the rim thickness measurements (Gardés et al. 2012; Franke and Joachim-Mrosko 2022).

Results of this study further show that at low water concentrations and identical P-T-t-X conditions, a small increase in the amount of water at the interface between the crystals (expressed in mg/m^2_{IF}) strongly enhances reaction rim growth rates until these reach a plateau value (Fig. 4; Table 1). The plateau values of two experimental series (dashed trendline in Fig. 5) that were performed at 1250 °C and 1300 °C show that the overall rim growth rate at the plateau decreases from ~− 14.40 m^2/s at 1300 °C to ~− 14.65 m^2/s at 1250 °C, which implies that rim growth rates decrease with decreasing temperature.

At rim growth rates of $<10^{-15}$ m^2/s the forsterite/enstatite (Fo/En) layer thickness ratio in double-layered rims is less than 3. Our results further show a steep increase in the
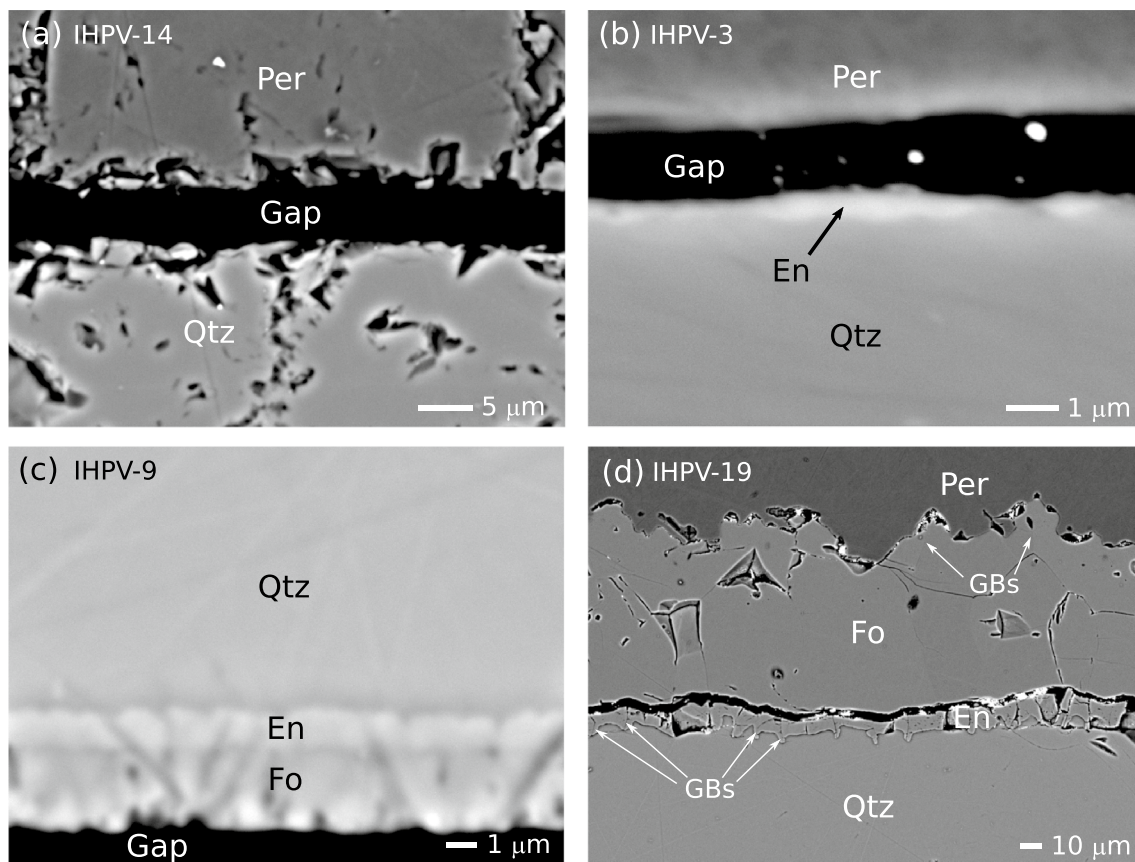
Fig. 3 Backscattered electron (BSE) images of reaction rims grown between single crystals of periclase and quartz ordered by increasing amount of water. **a** Oven-dried untreated single crystal experiment at 1300 °C lacking any sign of reaction. **b** Non-oven dried untreated single crystal experiment at 1100 °C showing the formation of a single-layered enstatite reaction rim with no sign of forsterite nucleation between enstatite and periclase. **c** Experiment at 1200 °C that contained an OH-doped periclase crystal as starting material. Water release during the experiment resulted in a maximum content of 40.8(91) mg/m^2_{IF} H_2O, which is the absolute amount of released water relative to the interface area. A double-layered forsterite-enstatite reaction rim with a Fo/En ratio of 2.25(17) developed. **d** Experiment at 1300 °C that contained brucite powder as starting material. Water release during the experiment resulted in a maximum content of 0.51 kg/m^2 H_2O. A double-layered forsterite-enstatite reaction rim with a Fo/En ratio of 7.19(38) developed. The forsterite-periclase and enstatite-quartz interfaces are wavy. The forsterite and enstatite rim widths shows maxima at positions where grain boundaries (GBs) are in direct contact with the reaction interface

reaction rim growth rate by more than 2 orders of magnitude while the relative forsterite/enstatite ratio increases by a factor of 4 (Table 1). However, overall rim growth rates show comparatively small fluctuations at values $>10^{-15}$ m^2/s while the relative Fo/En layer thickness ratio varies between between 3 and 12 (Fig. 6).

Discussion

Assessment of the experimental approach

Water present as OH-defect in periclase is initially not available as water that can potentially affect rim growth kinetics. The release rate of H_2O-related species from the doped periclase starting material must therefore be considered for the correct determination of the experimental duration (Joachim et al. 2013). This is particularly relevant for lower temperature experiments where diffusion rates are comparably sluggish. Therefore, the starting point for all experiments was defined as the moment when 90 wt% of H_2O were released from the OH-doped periclase. By choosing this number, we consider on one hand that more water will be released during the course of the experiment. Furthermore, while the absence of water-related species in the starting materials and/or reaction products after experiments IHPV-6 and 9 confirms that all water has left the doped periclase crystal and must have been available to potentially affect reaction rim growth, release rates were determined in furnace experiments that do not consider increasing partial H_2O pressure in the capsule. This might have led to a decrease of the H_2O release rate during the course of the experiments.
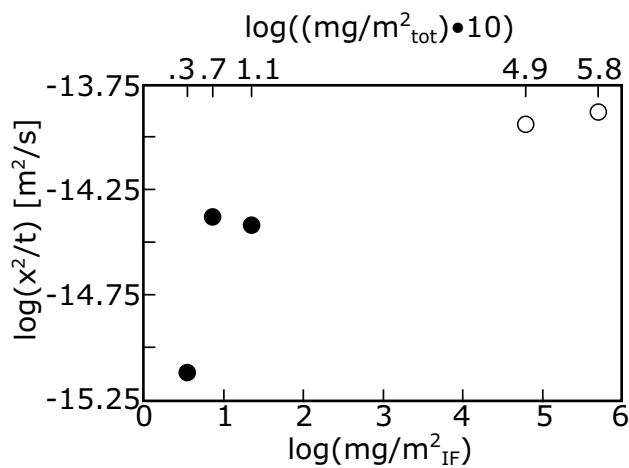
Fig. 4 Reaction rim growth rates of all experiments performed at a constant temperature of 1300 °C for 168 h (Table 1) versus the potential maximum water content normalized to the initial reaction interface between periclase and quartz (lower x-axis; $\log(mg/m^2_{IF})$) and the total sample surface area (upper x-axis; $\log((mg/m^2_{tot})\cdot10)$); for details see discussion. A steep increase in growth rates marks regime 2 at low water abundances until a plateau is reached between 7.35(98) and at least 22.4(28) mg/m^2_{IF} with growth rates of $10^{-14.38(6)}$ and $10^{-14.42(5)}$ m^2/s, respectively, which is related to regime 3 kinetics. At high water contents of 0.06 and 0.51 kg/m^2 a slow increase can be observed, which can be related to regime 4 kinetics (open symbols). Reaction rim growth of these data points may either be transport or interface controlled. Growth rates are expressed in m^2/s for comparison with literature values (Fig. 5)

Both aspects would result in an overestimation of the experimental duration. On the other hand, rim growth might start before 90 wt% of H_2O are released which would result in an underestimation of the experimental duration. Therefore, this approach is still only a reasonable approximation of the actual experimental duration. However, at 1300 °C, over 90% of the water is released within 3.5 h and 99% within 8 h in furnace experiments (Fig. 2). This means that an uncorrected experimental duration or release of 99 wt% H_2O as a starting point would affect determined growth rates by no more than a hundredth of an order of magnitude if compared to the chosen starting point, which is the release of 90% H_2O (Fig. 2, and Online Resource 3). Even the reaction rim growth rate of experiment IHPV-6 performed at 1100 °C changes from $10^{-17.29(3)}$ m^2/s when corrected for the time of 90 wt% H_2O release to $10^{-17.67(3)}$ m^2/s without this correction and to $10^{-16.80(3)}$ if 99 wt% release is considered. This is less than half an order of magnitude difference and thus small compared to the variations caused by differences in the maximum water per surface area concentrations. Another aspect that must be considered is that elemental transport across the rim is dominated by grain boundary diffusion (Gardés et al. 2012). The absolute surface area and, as a consequence, the available accommodation space for water depends on the overall rim thickness and the grain size,
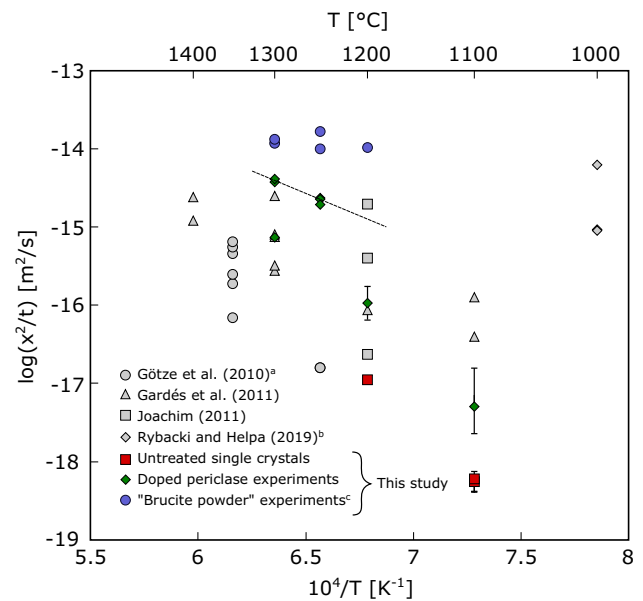

Fig. 5 Compilation of experimentally determined overall rim growth rates (Table 1) of forsterite-enstatite double-layered rims growing between periclase and quartz vs. inverse temperature. The dashed line connects experiments that were conducted with varying water contents but resulted in identical rim growth rates at a constant temperature, thus implying that rim growth in these experiments was taking place at regime 3 kinetics (Fig. 7). All datapoints below this dashed line represent experiments performed at water-undersaturated conditions at the grain boundaries (regime 2 kinetics), while all datapoints above this line represent regime 4 kinetics. For experiments with doped periclase crystals the error bars represent the growth rate corrected for the release time of H_2O at 0% H_2O release (lower limit) and 99% H_2O release (upper limit, see discussion for details). The error of other growth rates in this study are within the symbol size. [a]Results from run Exp.8 from Götze et al. (2010) were excluded from the dataset as they were deemed anomalously high. [b]For experiments conducted by Rybacki and Helpa (2019), only those with a differential stress of 0 were included. [c]Growth rates of the brucite series either plot in regime 4a or 4b and may either follow a parabolic growth law (m^2/s) or a linear rate law (m/s) (see text for details)

which both increase during the course of the experiment (Gardés et al. 2011). Consequently, the amount of water per grain boundary surface area might vary as rim growth proceeds while the absolute amount of water in the capsule remains constant. This is particularly relevant for single crystal experiments, which aim to minimize the surface area at the start of the experiment. To test the impact of these effects on determined average growth rates, we performed experiments at 1100 °C over a duration of 4 (IHPV-3) and 7 (IHPV-5) days. The observed rim thicknesses of 0.44(7) and 0.60(12) µm correspond within uncertainty to identical growth rates of $10^{-18.25(14)}$ and $10^{-18.23(16)}$ m^2/s, respectively. "Dry" single crystal experiments at 1300 °C performed by Gardés et al. (2011) with run durations of 5 min (Exp. PC27) and 24 h (Exp. PC16) show a decrease in growth rates from $10^{-14.63}$ to $10^{-15.58}$ m^2/s while growth rates of their 1100 °C
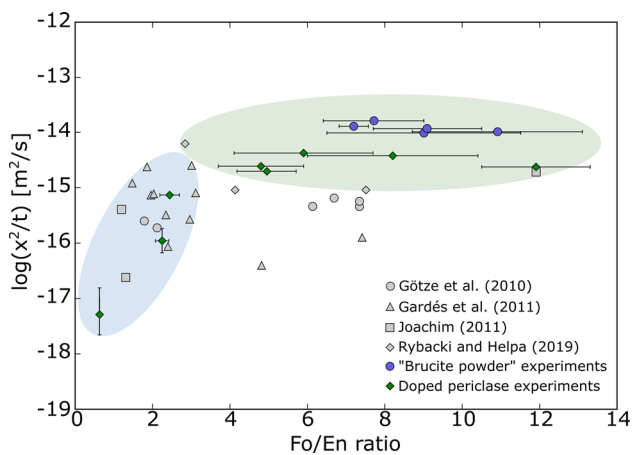
Fig. 6 Compilation of forsterite/enstatite rim thickness ratios in reaction rims grown between single crystals of quartz and periclase versus overall rim growth rate. There is a clear distinction between water-undersaturated (blue) regime 2, and water-saturated (green) regime 3 kinetics. Results from run Exp.8 from Götze et al. (2010) were excluded from the dataset. For experiments conducted by Rybacki and Helpa (2019) only those with a differential stress of 0 were included

experiments increase from $10^{-16.42}$ to $10^{-15.93}$ m²/s in the 3 h (Exp. PC23) and 72 h (Exp. PC20) runs, respectively. This implies that surface area variations during rim growth in experimental studies that produce rim thicknesses in the µm-scale and run for minutes to maximum days have only a minor effect on the determined average rim growth rates.

A new internal calibration for fluid-mediated reaction rim growth experiments

It is well established that grain boundary diffusion plays an important role in mediating reaction rim growth especially in relatively "dry" systems, where the water saturation state of grain boundaries controls the diffusivity (Farver and Yund 1995; Carlson 2010; Gardés et al. 2012). A common misconception in these studies is the assumption of a direct correlation between intergranular mass transport and the fluid-rock fraction. Within the capsule, potential sites where H-related species may be accommodated are solid–solid interfaces, (micro)cracks, grain boundaries and OH-defects in nominally anhydrous minerals (NAMs). If grain boundaries serve as dominant pathways for elemental transport across the rim, their characteristics and density need to be considered while the fluid-rock fraction also depends on H_2O solubilities and the diffusivities of H-bearing species in the grains' interiors. To determine the speciation of H-bearing compounds at those grain and phase boundaries that serve as main transport pathways for components across the rim, it is necessary to understand

the mechanisms how minute amounts water and other volatile components affect transport properties along different types of grain and phase boundaries. In a next step, the relation between this "active water" (water in the rim that actively catalyses intergranular mass transport and thus directly affects rim growth kinetics), and the relative water content (fluid-rock fraction) should be investigated, which will then allow us to unravel the fluid-history of a metamorphic or metasomatic rock.

In a first step to obtain a meaningful measure for the effect of water on reaction kinetics, an internal calibration to our experimental data is applied, which considers that only water available at surface areas can potentially affect the transport properties of grain and phase boundaries. To do this, the amount of water is expressed relative to a unit that scales with the grain boundary surface area, which is the interface area of the starting materials where reaction rim growth initiates. If it is assumed that all water released from the doped periclase or brucite is present and homogeneously distributed at this surface area, we can provide a theoretical maximum amount of active water per surface area for each experiment (mg/m^2_{IF}). This new internal calibration allows a precise control of the maximum amount of water per surface area by modifying the thickness of the OH-doped periclase crystal. A change of the dimensions of the interface area will always be proportional to the volume of the periclase crystal, so that any modification in its x–y-dimensions does not change the potential maximum amount of active water per surface area. This implies that only the initial OH-defect concentration and thickness of the doped periclase crystals need to be considered. By using OH-doped periclase crystals with varying OH-defect concentrations and thicknesses, we are thus able to provide an internally calibrated semi quantitative dataset, in which the maximum amount of available potentially active water per surface area expressed as H_2O-equivalent at the start of each experiment can be controlled and calculated even for water-undersaturated conditions (Table 1). However, the exact location of water in the capsule during the experiments remains still uncertain. The upper x axis in Fig. 4 shows the absolute amount of water relative to the total sample surface area of the starting materials in each experiment (mg/m^2_{tot}) while the lower x axis shows the absolute amount of water relative to the interface area (mg/m^2_{IF}) which represents the potential maximum amount of water at the grain boundaries. The nearly identical relative differences among individual data points on both x-axes suggest that we can use the relative difference of the potential maximum water per total surface area also as a measure for relative differences between individual experiments. Note that this can only be used as an internal calibration for the experimental setup used in this particular study.

Reaction rim growth from anhydrous to water-saturated conditions: the effect of water on mass transfer kinetics revisited

Rim growth at anhydrous conditions

The driest experiment that used undoped periclase as starting material and was oven dried before the capsule was sealed (IHPV-14) is the only experiment in which no reaction rim was detected (Fig. 3a). A possible explanation is that any adsorbed water that remained in the capsule was insufficient to catalyse nucleation of the product phases. This is supported by findings in similar rim growth experiments between monticellite and wollastonite (Joachim et al. 2012), where TEM images showed that reaction products were only found sporadically as isolated lenses, while at most places, no reaction rim could be observed. The occurrence of localised isolated lenses of the expected product phases were attributed to the presence of local fluid inclusions incorporated in the natural wollastonite reactant. This would suggest that a minimum water threshold is needed to initiate net-transfer reactions. However, absence of dissolution of the educts or transport of dissolved ions at extremely dry conditions cannot be ruled out. Nevertheless, these findings imply that geological samples may remain out of equilibrium for geological time scales at extremely dry conditions even if only NAMs are involved in the metamorphic reaction. This is further supported by recent natural observations, which showed that relict, anhydrous porphyroblasts may remain metastable at very dry conditions for geological timescales (Tursi 2022).

Rim growth at water-undersaturated conditions to water-saturated conditions: the effect of minute amounts of H_2O

The reaction progress during rim growth can be regarded as a three-step process, which is initiated by (i) product phase nucleation, followed by (ii) an interface reaction that controls rim growth rates at the onset of rim formation, and subsequently followed by (iii) diffusion-controlled processes (Abart and Petrishcheva 2011). Based on the concept of local equilibrium at all phase boundaries we would expect for example between periclase and quartz the formation of a double-layered Per|Fo|En|Qtz rim. However, in experiments that contained undoped periclase as starting material and were not oven dried before sealing, single-layered enstatite reaction rims formed but no forsterite layer could be detected between enstatite and periclase (Fig. 3b). This implies that the surface water that remained adsorbed in these samples is likely sufficient to catalyse the nucleation of enstatite but not of forsterite. This suggests that a minimum water threshold is not only required to initiate nucleation of all product

phases but might also vary between different product phases. Consequently, this may also imply that a layer sequence in a reaction rim that complies with local equilibrium at the individual phase boundaries is only observed, if the water threshold is higher than the minimum water threshold required for the nucleation of all respective product phases.

The formation of a double-layered Fo|En rim between Per and Qtz in experiments, in which water was introduced through OH-doped periclase crystals or brucite powder, is concordant with previous studies (Götze et al. 2010; Gardés et al. 2011, 2012; Rybacki and Helpa 2019) and indicates, based on the concept of local equilibrium, that the H_2O threshold to initiate re-equilibration was met. Enstatite rim growth rates using undoped periclase as starting material at 1100 °C were determined as $10^{-18.25(14)}$ and $10^{-18.23(16)}$ m^2/s (Table 1). These experiments are directly comparable to "dry" single crystal experiments performed at 1100 °C by Gardés et al. (2011). In that study, reaction rims with the sequence Per|Fo|En|Qtz grew at rates of $10^{-16.42}$ and $10^{-15.93}$ m^2/s. A potential explanation for the difference between the two studies is a minor variation in the addition of adsorbed surface water to the sample caused by small differences in the capsule preparation procedure and the use of a different experimental devices. This is supported by the fact that the experiment that contained a maximum amount of water per surface area of 3.49(19) mg/m$^2_{IF}$ H_2O with a growth rate of $10^{-15.12(3)}$ m^2/s and the "dry" single crystal piston cylinder experiments of Gardés et al. (2011) with a mean growth rate of $10^{-15.19(31)}$ m^2/s are similar, which further illustrates how extremely small variations in the abundance of active water may have a profound effect on rim growth kinetics.

In the 1300 °C series, reaction rims grown with a maximum amount of water per surface area ranging between 7.35(98) and 22.4(28) mg/m$^2_{IF}$ show within uncertainty identical growth rates of $10^{-14.38(6)}$ and $10^{-14.42(5)}$ m^2/s, respectively (Table 1, Fig. 4). This plateau, in which variations in water abundance do not affect overall rim growth rates, agrees well with regime 3 kinetics that is described as element transport across the rim along fluid-saturated grain boundaries (Gardés et al. 2012). Such a plateau is also present in the series performed at 1250 °C with the amount of water per surface varying between 3.40(19) and 24.0(43) mg/m$^2_{IF}$ while growth rates cluster between $10^{-14.61(5)}$ and $10^{-14.70(3)}$ m^2/s (Table 1). This implies that the dashed line in Fig. 5, which connects both plateaus, can be interpreted as visualization of the temperature dependence of the overall rim growth rate of a Fo|En rim growing between Per and Qtz at regime 3 kinetics. It has been shown that growth of this particular rim sequence is transport controlled for regime 3 kinetics and below (Gardés et al. 2012), which implies that all reaction rim growth rates that fall on or below this line follow a parabolic

growth pattern that is expressed as m^2/s in Fig. 5. All datapoints that plot above this line may either be transport controlled or interface controlled. In case of the latter, rim thickness would increase linearly with time. This implies that all datapoints above the dashed line in Fig. 5 might not follow a parabolic growth rate and were inserted only for comparison reasons. However, this allows us to visualize that these particular datapoints can be assigned to regime 4, which is only valid, because experimental durations remained constant in this study (Table 1). In fact, overall rim growth rates in all experiments that contain brucite powder as source of water plot consistently above the dotted line, thus indicating regime 4 kinetics (Fig. 5). Similar reaction rim growth experiments between crystals of periclase and quartz at water-saturated conditions from literature follow this trend when extrapolated to lower temperatures (Joachim 2011; Rybacki and Helpa 2019).

If we further assume that nucleation is hindered at anhydrous conditions (see section above), this implies that all datapoints that are below the dashed line in Fig. 5 represent water-undersaturated conditions at the grain boundaries (regime 2). To date, it has been assumed that the water-undersaturated regime 2 is effectively represented by a more or less instantaneous jump from 'dry' to 'wet' conditions and is difficult to experimentally register (Gardés et al. 2012). If correct, this would imply that all determined growth rates in this study stemming from experiments that used OH-doped periclase as starting material are the first experimentally produced reaction rims at regime 2 kinetics. However, experimental data from comparable experimental studies that performed re-equilibration experiments with 'dry' setups (Götze et al. 2010; Gardés et al. 2011; Joachim 2011) cover a broad range of growth rates and agree well with the range of growth rates covered by regime 2 kinetics in this study (Fig. 5). This strongly suggests, that the "dry" regime proposed in previous models (Gardés et al. 2012) in fact represents water-undersaturated conditions at the grain boundaries (regime 2) and not anhydrous conditions. The overall rim growth rate is extremely sensitive to very small water variations at water-undersaturated conditions. For example, growth rates vary by more than one order of magnitude below a maximum water content per surface area of 30 mg/m$^2_{IF}$ at 1300 °C. The growth rate variations covered by regime 2 kinetics increase towards lower temperatures (Fig. 5), presumably owing to a greater activation energy at water-undersaturated conditions compared to water-saturated conditions. This implies that for any rock assemblage that is subject to lower temperatures than our experimental conditions, presence or absence of minute amounts of water is likely to be a deciding factor if any significant re-equilibration takes place over geological timescales.

An advanced model of how water affects reaction kinetics

Results presented in this study diminish the gap between 'dry' and 'wet' kinetics and favour the idea that most formally labelled "dry" single crystal experiments represent in fact regime 2 kinetics while nucleation of product phases is inhibited at anhydrous regime 1 conditions. This demands a modification of our current understanding of the effect of water on rim growth kinetics. Therefore, a revised model of the classification presented in Gardés et al. (2012) is proposed. The modified model aims to illustrate the correlation between "active water", rim growth rates, transport pathways, and the different mechanisms that control re-equilibration. As a prerequisite, it is assumed that grain boundaries serve as main transport pathways for component transport through the reaction rim. If this is the case, then the water–rock fraction is not an ideal expression for the effect of water on reaction kinetics as this measure does not consider parameters such as the grain size, the grain boundary characteristics (e.g., Furstoss et al. 2022) or the pore space distribution in the product phases in the reaction rim. A more meaningful measure is to express component transport through the rim as a function of "active water", which is all water in the system that actively catalyses intergranular mass transport and thus directly affects rim growth rates. Eventually, the objective will be to define a universal measure that describes the fluid saturation state of an intergranular medium, which can be coupled to the transport pathway mechanism, and can be applied to different chemical systems. In water-undersaturated systems, "active water" may be described by hydrous species such as OH-groups, while the presence of molecular water is only expected at water-saturated conditions. However, not all grain boundaries may serve as fast pathways for component transport across the rim due to potential differences in their individual properties for example controlled by the grain misorientation, so that the terms "water activity" and "active water" are not necessarily identical. Our revised model is presented in Fig. 7 and includes the following regimes:

(1) Nucleation threshold: To initiate re-equilibration, a minimum water threshold has to be met, which is defined as the nucleation threshold. Below this threshold, water may be accommodated in any available accommodation space for H_2O-related species but nucleation of the product phases and therefore the reaction is inhibited.

(2) Water-undersaturated grain boundaries: once the nucleation threshold is overcome, the presence of H_2O-related species at the grain boundary immediately mediates transport of chemical components. The degree of undersaturation relative to a free fluid phase is best described by the amount of water at those grain
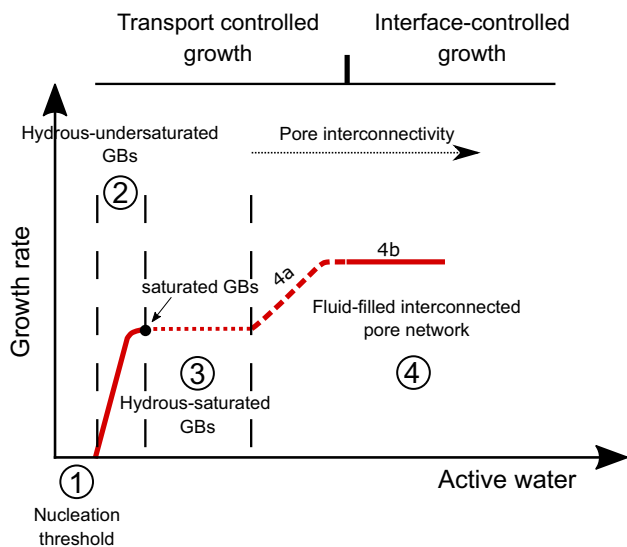
Fig. 7 Revised model visualizing the effect of water on reaction rim growth kinetics. The illustration shows the amount of "active water" present at the grain boundaries and/or in interconnected pores versus the overall rim growth rate. Regime 1: nucleation threshold, which is the minimum amount of water that is required to initiate metamorphic re-equilibration. Regime 2: hydrous-undersaturated grain boundaries, which describes mass transport in an intergranular medium at water-undersaturated conditions. In this regime, a minor variation in the abundance of active water can affect rim growth rates by orders of magnitude. Regime 3: hydrous saturated grain boundaries and isolated fluid-filled porosity: This regime lacks an interconnected fluid-filled pore network that may mediate mass transport. As a result, a plateau is expected in which the water abundance varies but not the growth rate as proposed by Gardés et al. (2012). The dotted line represents water in isolated pores that remains inactive until it suddenly becomes active when pores start to interconnect. Regime 4a: interconnected fluid-filled porosity I—Transport controlled growth: Fluid-filled pores start to interconnect, forming new potential pathways for mass transfer. Water in isolated pores remains inactive until the respective pore connects to the pore network. Regime 4b: interconnected fluid-filled porosity II—Interface-controlled growth: Eventually, the rate of mass transfer supersedes the potential interface-controlled growth rate at the reaction front

boundaries that contribute to elemental transport across the rim. The minimum amount of water at water-under-saturated conditions is greater than zero and marks the required amount of water to meet the nucleation threshold. In this regime, surface sites at the grain boundary are partly occupied with H_2O-related species. The degree of occupation is directly related to the amount of active water. In terms of kinetics, this regime is the most sensitive to small variations in the abundance of active water, so that bulk rock fluid content variations on the ppm level are often sufficient to affect growth rates by orders of magnitude.

(3) Water-saturated grain boundaries and isolated fluid-filled porosity: As the saturation point of the grain boundaries is reached, any additional water that enters

the system is distributed in the interstices of the granular aggregate (Watson and Brenan 1987). Free molecular water that is expelled into isolated pores does not automatically enhance mass transport as an interconnected network is lacking. This implies that the fluid–rock fraction can vary while rim growth rates are not affected. However, inactive water has the potential to serve as an active water proportion once the network is established (Gardés et al. 2012). This transition from "inactive" to "active" water is visualized by a dotted line in Fig. 7.

(4) Interconnected fluid-filled porosity I—Transport controlled growth: Fluid-filled pores start to form an interconnected, fluid-filled network which introduces new pathways for mass transfer. As the interconnectivity of fluid-filled channels increases, the proportion of active water rises continuously. The transition from regime 3 to regime 4 occurs when interconnected channels of molecular water start to contribute as fast pathways for elemental transport across the rim.

(5) Interconnected fluid-filled porosity II—Interface-controlled growth: Further development of the interconnected fluid-filled network increases the rate of mass transport across the rim until the mechanism that controls re-equilibration eventually transitions from transport-controlled to interface-controlled growth.

Rim-microstructures as a new physico-chemical gauge

In a multilayered rim sequence, any parameter that modifies the relative diffusivities of the rim growth controlling component(s) between the layers has a direct effect on the layer thickness ratios. In this study, we may assume that MgO is the component that dominantly controls the overall rim growth rate of the double-layered forsterite-enstatite reaction rim growing between periclase and quartz (Milke et al. 2001; Gardés and Heinrich 2011; Joachim et al. 2012). This implies that in a transport-controlled regime, the forsterite/enstatite thickness ratio is controlled by the relative bulk diffusivity of MgO in the forsterite and enstatite layer with increasing $D_{MgO}^{Fo}/D_{MgO}^{En}$ resulting in an increase of $\Delta x_{Fo}/\Delta x_{En}$. Results of this study combined with literature data show that rims that were growing at water-saturated conditions (regime 3 and 4) develop forsterite/enstatite thickness ratios of > 3 whereas all experiments that were water-undersaturated (regime 2) display forsterite/enstatite ratios of < 3 (Fig. 6). This implies that an increasing abundance of "active water" not only controls overall rim growth rates but also has a direct effect on the relative MgO-diffusivity along a forsterite grain boundary, which increases relative to the MgO diffusivity along an enstatite grain boundary.

Recent numerical simulations point toward the existence of anomalously high non-silicate oxygen sites in forsterite

grain boundaries (Furstoss et al. 2022). The high potential for these free oxygens to be protonated by dissociated water may provide an explanation for the increase in component diffusivities along grain boundaries catalysed by the presence of "active water". This would also explain why the effect of "active water" has a more pronounced effect on the diffusivity of MgO along forsterite grain boundaries compared to enstatite grain boundaries as the free oxygen density differs between the two phases. If correct, this would imply that the individual characteristic of each grain boundary affects its transport properties. The question arises whether grain boundaries of some phases have the capability to accommodate more "active water" than others. If this were to be the case, perhaps classifying the diffusivity versus the fluid–rock fraction is not only related to the grain size but also unique for each phase. Investigating the intrinsic differences between different grain complexions on the nano-scale (Cantwell et al. 2014) may provide further insights into the mechanism how "active water" affects the reaction kinetics.

Temperature is—as any other physico-chemical parameter affecting component diffusivities in geological systems—another parameter that might affect the layer thickness ratios in a multilayered reaction rim. In fact, it has been shown that the Fo/En thickness ratio increases with increasing temperature by a factor 4 between 1100 and 1400 °C (Gardés and Heinrich 2011). However, results of this study combined with literature data show that the effect of temperature on the relative Fo/En layer thicknesses is small compared to the effect of water (Fig. 6).

Another possible explanation that can affect the Fo/En thickness ratio are finite interface mobilities between the layers in multilayered reaction rim sequences. These may particularly become relevant in regime 4b kinetics.

In a broader context, the findings of this study imply that multilayered reaction rims have the potential to record the conditions of their formation through layer thickness ratios, which may be used as new physico-chemical gauges. This may offer an alternative approach to estimate the quantity of water present, in addition to previously discussed indicators such as rim roughness or rim structure (Milke et al. 2007; Joachim et al. 2019). In multi-component systems, effects of "active water" on the rim microstructure might even be more complex as bi- or even multimineralic layers can develop (Joachim et al. 2019), whose internal microstructure can potentially be linked to the "active water" content. This is of particular relevance for natural metamorphic and metasomatic samples that lost any direct information such as fluid inclusions. In these samples, the internal microstructure of reaction rims may potentially be used to decipher the availability and abundance of fluids at formation conditions. The combined analysis of relative layer thickness ratios and overall growth rate in a well-calibrated system gives natural reaction rims even the potential to estimate, only through the analysis of the rim microstructure and overall rim thickness, the duration of re-equilibration at those metamorphic conditions during which fluids infiltrated the host rock (Fig. 6). This requires experimental studies explicitly aiming at component diffusivities in the grain and phase boundaries in and between various materials and their dependence on relevant parameters such as temperature, fluid composition and abundance, bulk chemical composition, oxygen fugacity, the grain boundary characteristics, etc.

Conclusions

This study presents a new experimental approach that enables the introduction of defined minute amounts of water to an experimental sample by using OH-doped periclase as starting material. This allows to evaluate the role of H_2O on transport kinetics and as a direct consequence rim growth rates at water-undersaturated conditions. Based on the results of this study, the model proposed by Gardés et al. (2012) is revised. This revised model describes the rim growth rate as a function of "active water" and illustrates the complex correlation between the amount of water that may (i) actively catalyse rim formation, (ii) affect transport of the rim growth controlling component(s) across the rim, and (iii) modify the mechanisms that control overall rim growth. This classification includes four successive rim growth rate regimes: (1) Nucleation threshold (2) Water-undersaturated grain boundaries (3) Water-saturated grain boundaries and isolated fluid-filled porosity (4a) Interconnected fluid-filled porosity I—Transport controlled growth, and (4b) Interconnected fluid-filled porosity II—Interface-controlled growth.

Moreover, the following conclusions can be drawn:

– Water acts as a catalyst for metamorphic reactions and a minimum H_2O threshold is required to initiate metamorphic reaction.

– Re-equilibration rates between water-undersaturated and water-saturated systems (regime 2) may differ by multiple orders of magnitude at temperatures representative for lower crustal and upper mantle settings. This implies that in some chemical systems, the presence of H_2O-related species is a key requisite for any significant metamorphism to take place over geological timescales.

– Microstructures i.e. relative rim thickness ratios can be used to distinguish between net-transfer reactions that occurred in water-undersaturated and water-saturated systems, giving reaction rims the potential to be utilized as "geohygrometers".

– The trend of an increasing Fo/En rim thickness ratio as a function of rim growth rate at water-undersaturated conditions gives reaction rims the potential to estimate not only the composition and abundance of fluids present

during metamorphic re-equilibration at water-undersaturated conditions but also to determine the duration of those metamorphic events, during which these extremely small amounts of fluids infiltrated the host rock.

Data availability The authors confirm that the data supporting the findings in this study are available within the article and the supplementary materials (ESM_1-3).

Declarations

Conflict of interest The authors have no competing interests to declare that are relevant to the content of this article.

References

Abart R, Petrishcheva E (2011) Thermodynamic model for reaction rim growth: interface reaction and diffusion control. Am J Sci 311:517–527. https://doi.org/10.2475/06.2011.02

Abart R, Kunze K, Milke R, Sperb R, Heinrich W (2004) Silicon and oxygen self diffusion in enstatite polycrystals: the Milke et al. (2001) rim growth experiments revisited. Contrib Mineral Petrol 147:633–646. https://doi.org/10.1007/s00410-004-0596-9

Austrheim H (1987) Eclogitization of lower crustal granulites by fluid migration through shear zones. Earth Planet Sci Lett 81:221–232. https://doi.org/10.1016/0012-821X(87)90158-0

Brady J, McCallister R (1983) Diffusion data for clinopyroxenes from homogenization and self-diffusion experiments. Am Mineral 68:95–105

Cantwell PR, Tang M, Dillon SJ, Luo J, Rohrer GS, Harmer MP (2014) Grain boundary complexions. Acta Mater 62:1–48. https://doi.org/10.1016/j.actamat.2013.07.037

Carlson WD (2010) Dependence of reaction kinetics on H_2O activity as inferred from rates of intergranular diffusion of aluminium. J Metamorph Geol 28:735–752. https://doi.org/10.1111/j.1525-1314.2010.00886.x

Clark C, Schmidt Mumm A, Faure K (2005) Timing and nature of fluid flow and alteration during Mesoproterozoic shear zone formation, Olary domain, South Australia. J Metamorph Geol 23:147–164. https://doi.org/10.1111/j.1525-1314.2005.00568.x

Carter RE (1961) Mechanism of solid-state reaction between magnesium oxide and aluminum oxide and between magnesium oxide and ferric oxide. J Am Ceram Soc 44:116–120. https://doi.org/10.1111/j.1151-2916.1961.tb13724.x

Dohmen R, Milke R (2010) Diffusion in polycrystalline materials: grain boundaries, mathematical models, and experimental data. Rev Miner Geochem 72:921–970. https://doi.org/10.2138/rmg.2010.72.21

Farver JR, Yund RA (1995) Grain boundary diffusion of oxygen, potassium and calcium in natural and hot-pressed feldspar aggregates. Contrib Mineral Petrol 118:340–355. https://doi.org/10.1007/s004100050019

Fisher GW (1978) Rate laws in metamorphism. Geochim Cosmochim Acta 42:1035–1050

Fisler DK, Mackwell SJ, Petsch S (1997) Grain boundary diffusion in enstatite. Phys Chem Min 24:264–273. https://doi.org/10.1007/s002690050038

Franke M, Joachim-Mrosko B (2022) The effect of fluorine on reaction rim growth dynamics in the ternary $CaO-MgO-SiO_2$ system. Am Mineral 107:1477–1486. https://doi.org/10.2138/am-2022-8123CCBY

Furstoss J, Hirel P, Carrez P, Cordier P (2022) Complexions and stoichiometry of the 60.8°//[100](011) symmetrical tilt grain boundary in Mg2SiO4 forsterite: a combined empirical potential and first-principles study. Am Mineral. https://doi.org/10.2138/am-2022-8420

Gardés E, Heinrich W (2011) Growth of multilayered polycrystalline reaction rims in the $MgO-SiO_2$ system, part II: modelling. Contrib Mineral Petrol 162:37–49. https://doi.org/10.1007/s00410-010-0581-4

Gardés E, Wunder B, Wirth R, Heinrich W (2011) Growth of multilayered polycrystalline reaction rims in the $MgO-SiO_2$ system, part I: experiments. Contrib Mineral Petrol 161:1–12. https://doi.org/10.1007/s00410-010-0517-z

Gardés E, Wunder B, Marquardt K, Heinrich W (2012) The effect of water on intergranular mass transport: new insights from diffusion-controlled reaction rims in the $MgO-SiO_2$ system. Contrib Mineral Petrol 164:1–16. https://doi.org/10.1007/s00410-012-0721-0

González R, Chen Y (2002) Transport of hydrogenic species in crystalline oxides: radiation and electric-field-enhanced diffusion. J Phys Condens Matter 14:R1143–R1173. https://doi.org/10.1088/0953-8984/14/45/201

Götze LC, Abart R, Rybacki E, Keller LM, Petrishcheva E, Dresen G (2010) Reaction rim growth in the system $MgO-Al_2O_3-SiO_2$ under uniaxial stress. Mineral Petrol 99:263–277. https://doi.org/10.1007/s00710-009-0080-3

Incel S, Milke R, Wunder B (2022) Orthopyroxene rim growth during reaction of (Co, Ni, Mn, Zn)-doped forsterite and quartz: Experimental constraints on element distribution and grain boundary diffusion. Mineral Petrol 116:137–149. https://doi.org/10.1007/s00710-022-00773-3

Joachim B (2011) Reaction rim growth in the systems $MgO-SiO_2$ and $CaO-MgO-SiO_2$: diffusion pathways and the effect of water. Dissertation, German Research Centre of Geosciences, Potsdam

Joachim B, Gardés E, Abart R, Heinrich W (2011) Experimental growth of åkermanite reaction rims between wollastonite and monticellite: evidence for volume diffusion control. Contrib Mineral Petrol 161:389–399. https://doi.org/10.1007/s00410-010-0538-7

Joachim B, Gardés E, Velickov B, Abart R, Heinrich W (2012) Experimental growth of diopside + merwinite reaction rims: The effect of water on microstructure development. Am Mineral 97:220–230. https://doi.org/10.2138/am.2011.3819

Joachim B, Wohlers A, Norberg N, Gardés E, Petrishcheva E, Abart R (2013) Diffusion and solubility of hydrogen and water in periclase. Phys Chem Miner 40:19–27. https://doi.org/10.1007/s00269-012-0542-8

Joachim B, Heinrich W, Höschen C, Abart R (2019) The effect of H₂O fluid on relative component mobilities in a bimineralic reaction rim in the system CaO-MgO-SiO₂. Eur J Mineral 31:61–72. https://doi.org/10.1127/ejm/2019/0031-2796

Joesten R (1977) Evolution of mineral assemblage zoning in diffusion metasomatism. Geochim Cosmochim Acta 41:649–670. https://doi.org/10.1016/0016-7037(77)90303-9

Keller LM, Götze LC, Rybacki E, Dresen G, Abart R (2010) Enhancement of solid-state reaction rates by non-hydrostatic stress effects on polycrystalline diffusion kinetics. Am Mineral 95:1399–1407. https://doi.org/10.2138/am.2010.3372

Libowitzky E, Rossman GR (1997) An IR absorption calibration for water in minerals. Am Mineral 82:1111–1115. https://doi.org/10.2138/am-1997-11-1208

Liu M, Peterson J, Yund RA (1997) Diffusion-controlled growth of albite and pyroxene reaction rims. Contrib Mineral Petrol 126:217–223. https://doi.org/10.1007/s004100050245

Milke R, Heinrich W (2002) Diffusion-controlled growth of wollastonite rims between quartz and calcite: Comparison between nature and experiment. J Metamorph Geol 20:467–480. https://doi.org/10.1046/j.1525-1314.2002.00384.x

Milke R, Wiedenbeck M, Heinrich W (2001) Grain boundary diffusion of Si, Mg, and O in enstatite reaction rims: a SIMS study using isotopically doped reactants. Contrib Mineral Petrol 142:15–26. https://doi.org/10.1007/s004100100277

Milke R, Dohmen R, Becker HW, Wirth R (2007) Growth kinetics of enstatite reaction rims studied on nano-scale, Part I: Methodology, microscopic observations and the role of water. Contrib Mineral Petrol 154:519–533. https://doi.org/10.1007/s00410-007-0207-7

Milke R, Kolzer K, Koch-Müller M, Wunder B (2009) Orthopyroxene rim growth between olivine and quartz at low temperatures (750–950°C) and low water concentration. Mineral Petrol 97:223–232. https://doi.org/10.1007/s00710-009-0093-y

Milke R, Neusser G, Kolzer K, Wunder B (2013) Very little water is necessary to make a dry solid silicate system wet. Geology 41:247–250. https://doi.org/10.1130/G33674.1

Mindaleva D, Uno M, Higashino F, Nagaya T, Okamoto A, Tsuchiya N (2020) Rapid fluid infiltration and permeability enhancement during middle-lower crustal fracturing: evidence from amphibolite-granulite-facies fluid-rock reaction zones, Sør Rondane Mountains. East Antarctica Lithos 372–373:105521. https://doi.org/10.1016/j.lithos.2020.105521

Phillips BBA, Busing WR (1956) Comparison of the infrared and Raman spectra of some crystalline hydroxides. J Phys Chem 61:502

Putnis A, Austrheim H (2010) Fluid-induced processes: metasomatism and metamorphism. Geofluids 10:254–269. https://doi.org/10.1111/j.1468-8123.2010.00285.x

Rossi RC, Fulrath RM (1963) Epitaxial growth of spinel by the reaction in solid state. J Am Ceram Soc 46:145–149

Rubie DC (1986) The catalysis of mineral reactions by water and restrictions on the presence of aqueous fluid during metamorphism. Mineral Mag 50:399–415. https://doi.org/10.1180/minmag.1986.050.357.05

Rybacki E, Helpa V (2019) Influence of differential stress on the growth of wet enstatite and enstatite-forsterite reaction rims. Mineral Petrol 113:433–448. https://doi.org/10.1007/s00710-019-00667-x

Schorn S, Diener JFA (2017) Details of the gabbro-to-eclogite transition determined from microtextures and calculated chemical potential relationships. J Metamorph Geol 35:55–75. https://doi.org/10.1111/jmg.12220

Truckenbrodt J, Johannes W (1999) H₂O loss during piston-cylinder experiments. Am Mineral 84:1333–1335. https://doi.org/10.2138/am-1999-0909

Tursi F (2022) The key role of μH₂O gradients in deciphering microstructures and mineral assemblages of mylonites: examples from the Calabria polymetamorphic terrane. Mineral Petrol 116:1–14. https://doi.org/10.1007/s00710-021-00766-8

Watson EB, Brenan JM (1987) Fluids in the lithosphere, 1. Experimentally-determined wetting characteristics of CO2H2O fluids and their implications for fluid transport, host-rock physical properties, and fluid inclusion formation. Earth Planet Sci Letter 85:497–515. https://doi.org/10.1016/0012-821X(87)90144-0

Watson EB, Price JD (2002) Kinetics of the reaction $MgO + Al_2O_3 \rightarrow MgAl_2O_4$ and Al-Mg interdiffusion in spinel at 1200 to 2000°C and 1.0 to 4.0 GPa. Geochim Cosmochim Acta 66:2123–2138. https://doi.org/10.1016/S0016-7037(02)00827-X

Whitney WP, Stubican VS (1971) Interdiffusion studies in the system MgOAl₂O₃. J Phys Chem Solids 32:305–312. https://doi.org/10.1016/0022-3697(71)90015-1

Yund RA (1997) Rates of grain boundary diffusion through enstatite and forsterite reaction rims. Contrib Mineral Petrol 126:224–236. https://doi.org/10.1007/s004100050246

Zaraysky G, Balashov V, Lebedeva M (1989) Macrokinetic model of metasomatic zonality. Geokhimiya 10:1386–1395